

# Vibrational behavior of the $M_{n+1}AX_n$ phases from first-order Raman scattering ( $M = \text{Ti, V, Cr}$ , $A = \text{Si}$ , $X = \text{C, N}$ )

Jonathan E. Spanier,\* Surojit Gupta, Maher Amer,† and Michel W. Barsoum

Department of Materials Science and Engineering, Drexel University, Philadelphia, Pennsylvania 19104, USA

(Received 24 June 2004; revised manuscript received 3 September 2004; published 21 January 2005)

We report on the Raman spectra of  $\text{Ti}_3\text{SiC}_2$  (312),  $M_2\text{AlC}$  (211) ( $M = \text{Ti, V, Cr, and Nb}$ ) and  $\text{Ti}_4\text{AlN}_3$  (413), as representative compounds from the family of  $M_{n+1}AX_n$  phases. Intense and narrow first-order Raman peaks are observed, and we present an analysis of the spectra based on symmetry considerations and from results of first-principles calculations of phonon frequencies. The agreement between experimental and calculated mode energies is excellent. The identification of the modes enables application of Raman scattering as a diagnostic tool for the detailed study of the structural and physical properties of this family of compounds and their engineered solid solutions.

DOI: 10.1103/PhysRevB.71.012103

PACS number(s): 78.30.-j, 63.20.Dj, 71.15.Mb

Recently, seemingly unrelated layered solids such as graphite, ternary carbides and nitrides (see below), hexagonal BN, ice, and most importantly, mica—and thus much of geology—were all classified as kinking nonlinear elastic (KNE) solids.<sup>1</sup> These solids all deform by the formation of dislocation-based incipient kink bands (IKB's), that are fully reversible, that give way to mobile dislocation walls, which in turn collapse into kink boundaries.<sup>2</sup> Furthermore, it was shown that the hysteretic mesoscopic units—invoked to explain the behavior of nonlinear mesoscopic elastic solids<sup>3,4</sup>—are nothing but IKB's. Understanding the behavior of KNE solids is thus important in geology, the behavior of graphite, as well as a new class of layered ternary carbides and nitrides, viz., the *MAX* phases.

The so-called *MAX* phases [ $M_{n+1}AX_n$ , where  $n \geq 1$ ,  $M$  is an early transition metal,  $A$  is an A-group (mostly IIIA, IVA) element, and  $X$  is C or N] have recently attracted considerable attention due to their unusual physical, mechanical, and thermal properties.<sup>5,6</sup> In all these compounds, near-close-packed transition metal carbide and/or nitride layers are interleaved with layers of pure A-group element. When  $n = 1$ , e.g.,  $\text{Ti}_2\text{AlN}$  (hereafter referred to as 211), every *third* layer is an A-group element layer (Fig. 1); for  $n = 2$  (312), every *fourth* layer (Fig. 2); for  $n = 3$  (413), every *fifth* layer. There are over fifty 211 compounds, at least three 312 compounds, and one 413, namely,  $\text{Ti}_4\text{AlN}_3$ .<sup>5,6</sup>

Though the Raman spectrum of  $\text{Ti}_3\text{SiC}_2$  has been reported previously,<sup>7</sup> tentative assignments of atoms involved with a few of the observed modes were made therein on the basis of comparison with  $\text{TiC}_{0.67}$ . The purpose of this paper is to present the 300 K Raman spectra of *MAX* phase compounds selected to represent each of the three stoichiometries, along with *ab initio* calculations and symmetry analysis for these solids, thus permitting the definitive identification of the observed Raman peaks. The understanding of these modes, especially the shear modes, should lead to a much better understanding of IKB's and in turn the deformation of KNE's.

Fully dense, predominantly single phase samples of  $\text{Cr}_2\text{AlC}$  (Ref. 8),  $\text{Ti}_2\text{AlC}$  (Ref. 9),  $\text{V}_2\text{AlC}$  (Ref. 10),  $\text{Ti}_4\text{AlN}_3$  (Ref. 11), and  $\text{Nb}_2\text{AlC}$  (Ref. 12) were made by

reactively hot isostatic pressing the appropriate stoichiometric mixtures of powders of the constituent elements and/or appropriate carbides. The  $\text{V}_2\text{AlC}$  samples contained some relatively large platelike grains. The samples were fractured to expose  $\approx 2 \times 2 \text{ mm}^2$  basal planes that were studied.

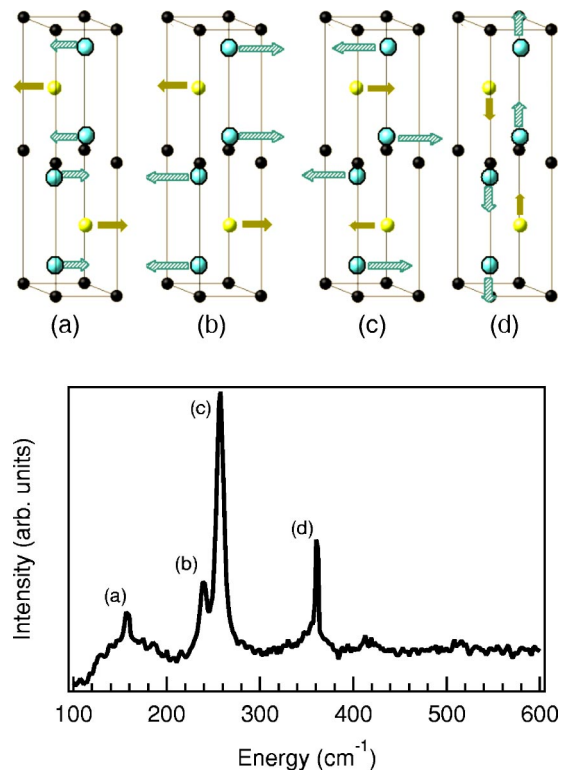


FIG. 1. (Color online) Raman spectrum collected within a single grain of  $\text{V}_2\text{AlC}$ . The measured, Lorentzian-fitted energies are approximately (a) 158, (b) 239, (c) 258, and (d) 360  $\text{cm}^{-1}$ . Shown above the plot are schematics of the corresponding atomic displacements for the Raman-active phonons in the 211 unit cell for  $\text{V}_2\text{AlC}$ . The C atoms are denoted by black spheres; the V atoms are encircled and blue (light gray) and occupy sites in every other elemental atomic plane. The Al atoms are denoted in yellow (off-white), and occupy sites in every third plane.

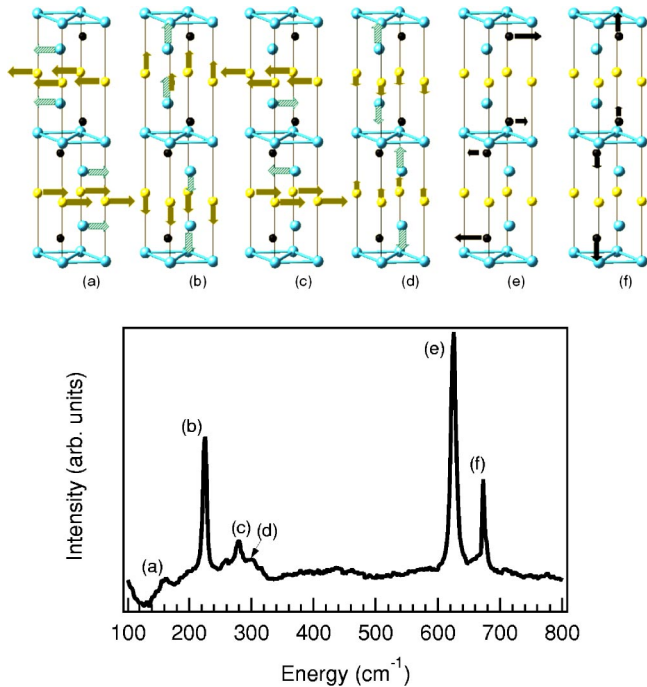


FIG. 2. (Color online) Raman spectrum collected within a single grain of  $\text{Ti}_3\text{SiC}_2$ . The measured, Lorentzian-fitted energies are approximately (a) 159, (b) 226, (c) 279, (d) 301, (e) 625, and (f) 673  $\text{cm}^{-1}$ . Shown above the plot are schematics of the corresponding atomic displacements for the Raman-active phonons in the  $\text{Ti}_3\text{SiC}_2$  unit cell. The C atoms are denoted by black spheres; the Ti atoms are blue (gray) with light blue (light gray) arrows, and occupy sites in every other elemental atomic plane. The Si atoms appear as yellow (off-white) spheres with dark yellow (dark gray) arrows, and occupy sites in every fourth plane.

The  $\text{Ti}_3\text{SiC}_2$  samples were made using a sinter forging technique.<sup>13</sup> The resulting samples also had large platelike grains with diameters of 1 to 2 mm and thicknesses of the order of 200  $\mu\text{m}$ .

Unpolarized Raman scattering was collected at 300 K from within single grains of  $\text{V}_2\text{AlC}$  and  $\text{Ti}_3\text{SiC}_2$  and from polycrystalline samples of the other 211 phases and  $\text{Ti}_4\text{AlN}_3$ . HeNe laser excitation (543.5 nm) was focused to a spot size of  $\sim 4 \mu\text{m}$  with an incident power of  $\sim 12 \text{ mW}$ . The spectra were collected in the backscattering configuration  $z(x, x+y)\bar{z}$  ( $x$  is arbitrary with respect to the axes in the basal plane,  $z \parallel c$ -axis); using a Renishaw 2000 spectrometer with an air-cooled CCD array detector. All experimental peak energies and linewidths reported were obtained from multiple-peak Lorentzian fitting, and the experimental resolution of the peak positions is within 1–2  $\text{cm}^{-1}$ .

Phonon energies were calculated based on first-principles calculations of total energy, Hellman-Feynman forces, and the dynamical matrix using VASP (Ref. 14) and PHONON (Ref. 15) as implemented within MedeA.<sup>16</sup> Here the Kohn-Sham equation is solved using projector augmented wave<sup>17,18</sup> (PAW) potentials and the generalized gradient approximation<sup>19</sup> (GGA). The summation is constrained to a  $3 \times 3 \times 3$   $k$ -point mesh. The structures were optimized while

TABLE I. Lattice and structural parameters (Ref. 20–22) used in calculations of phonon energies. The values listed are the result of calculations of energy-minimized structures using VASP (Ref. 14).  $z_M$  denotes the  $M$ -element atomic positions normalized to each lattice parameter  $c$ . Following the Wyckoff notation, these atoms occupy the  $4f$  sites for the 211 and 312 structures; in the 413 structure, the  $\text{Ti}_I$ ,  $\text{Ti}_{II}$ , and  $\text{N}_{II}$  occupy the  $4f$ ,  $4e$ , and  $4f$  sites, respectively.

	$\text{V}_2\text{AlC}^a$	$\text{Ti}_2\text{AlC}^a$	$\text{Cr}_2\text{AlC}^a$	$\text{Nb}_2\text{AlC}^a$	$\text{Ti}_3\text{SiC}_2^b$	$\text{Ti}_4\text{AlN}_3^c$
$a$ ( $\text{\AA}$ )	2.950	3.060	2.850	3.100	3.0575	2.988
$c$ ( $\text{\AA}$ )	13.290	13.670	12.720	13.800	17.6235	23.372
$z_M$	0.0840	0.0837	0.0847	0.0830	0.0727	0.0542 ( $\text{Ti}_I$ ) 0.1547 ( $\text{Ti}_{II}$ ) 0.1050 ( $\text{N}_{II}$ )

<sup>a</sup>Reference 20

<sup>b</sup>Reference 21.

<sup>c</sup>Reference 22.

maintaining the constraints imposed by the space-group symmetry elements using calculated lattice parameters reported previously (see Table I).<sup>20–22</sup> For the phonon calculations, nonequivalent atoms positions for each of the structures were used to generate rhombohedral supercells consisting of 24, 36, and 48 atoms for the 211, 312, and 413 structures, respectively. In these supercells, the internal degrees of freedom were relaxed while the lattice parameters were fixed.

The MAX phases are a member of the space group  $D_{6h}^4$  ( $P_6^3/mmc$ ). For the 211 structures, there are a total of 24 modes. In addition to the three acoustic modes ( $A_{2u} + E_u$ ), there are four Raman-active optical modes, three of which are Raman-active ( $A_g + 2E_{2g}$ ) and one which is both Raman-active and infrared-active ( $E_g$ ). For  $\text{Ti}_3\text{SiC}_2$ , there are seven ( $2A_g + 2E_g + 3E_{2g}$ ) Raman-active modes of the 33 total optical modes, two of which are also infrared-active. Finally, for  $\text{Ti}_4\text{AlN}_3$  there are a total of 10 modes ( $3A_g + 3E_g + 4E_{2g}$ ), three of which are also infrared-active.

The 300-K Raman spectra of a single grain of  $\text{V}_2\text{AlC}$  and  $\text{Ti}_3\text{SiC}_2$  are shown in Figs. 1 and 2 respectively. The spectrum of a polycrystalline sample of  $\text{Ti}_4\text{AlN}_3$  is shown in Fig. 3. For  $\text{V}_2\text{AlC}$ , four distinct sharp peaks are observed at

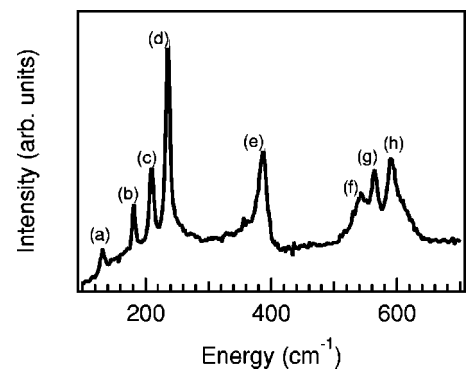


FIG. 3. Raman spectrum of  $\text{Ti}_4\text{AlN}_3$ . The measured, Lorentzian-fitted energies are approximately (a) 132, (b) 181, (c) 208, (d) 235, (e) 386, (f) 539, (g) 563, and (h) 592  $\text{cm}^{-1}$ .

TABLE II. Measured Lorentzian-fitted Raman peak energies  $\omega_{\text{expt}}$  and full-width half-maximum linewidths  $\Gamma$  in  $\text{cm}^{-1}$ , and corresponding calculated peak energies and symmetries for selected 211 aluminum carbides. In the table, the asterisk refers to a mode that could not be clearly discerned in the experimental spectrum.

mode	$\text{V}_2\text{AlC}$			$\text{Nb}_2\text{AlC}$			$\text{Ti}_2\text{AlC}$			$\text{Cr}_2\text{AlC}$			Irrep.
	$\omega_{\text{expt}}$	$\Gamma$	$\omega_{\text{calc}}$	$\omega_{\text{expt}}$	$\Gamma$	$\omega_{\text{calc}}$	$\omega_{\text{expt}}$	$\Gamma$	$\omega_{\text{calc}}$	$\omega_{\text{expt}}$	$\Gamma$	$\omega_{\text{calc}}$	
(a)	157.5	4.9	145	149.4	15	148	149.9	12.9	149	150.9	19.9	156	$E_{2g}$
(b)	239.7	4.0	244	$\sim 211$	24	197.7	268.1	9.5	262	246.3	7.3	247	$E_g$
(c)	257.2	5.3	248	$\sim 190$	29	181.5	262.1	5.8	248	*	-	237	$E_{2g}$
(d)	361.2	4.4	361	262.8	15	268.3	365.1	12.4	387	339.2	7.6	345	$A_g$

approximately 158, 240, 257, and 361  $\text{cm}^{-1}$ , and weaker peaks near 413, 509, and 693  $\text{cm}^{-1}$ . The calculated phonon energies for the four first-order Raman active modes in  $\text{V}_2\text{AlC}$  Raman-active are listed in Table II. The lattice distortions associated with each of these observed Raman-active modes are shown schematically above the plot in Fig. 1. The results for fitted peak positions, linewidths, and calculated energies for three other 211 phases are listed in Table II along with those for  $\text{V}_2\text{AlC}$ . We note that in  $\text{V}_2\text{AlC}$  the calculated mode energy for displacements shown in Fig. 1(c) is slightly higher than that for Fig. 1(b). However, for each of the three other 211 structures, the calculated mode energy associated with the atomic displacements shown in 1(c) is actually lower ( $\sim 5\text{--}10\%$ ) than that of 1(b).

For  $\text{Ti}_3\text{SiC}_2$ , the measured spectrum (Fig. 2) shows five distinct peaks at approximately 159, 226, 279, 625, and 673  $\text{cm}^{-1}$ , along with two weak peaks at approximately 260 and 301  $\text{cm}^{-1}$ . The corresponding lattice distortions are shown in Figs. 2(a)–2(f). The calculated mode energies compare quite well with measured peak energies as shown in Table III. The measured peaks near 159 and 226  $\text{cm}^{-1}$  are shear and longitudinal vibrations involving the Si and Ti atomic planes, respectively. The mode near 279  $\text{cm}^{-1}$  involves shear vibrations of the Si atomic planes with antiparallel shear of the adjacent Ti atomic planes. The mode near 301  $\text{cm}^{-1}$  involves longitudinal vibrations of the Si atomic planes with antiparallel dilatation of the adjacent Ti atomic planes. Modes at 625 and 673  $\text{cm}^{-1}$  are of  $E_{2g}$  and  $A_g$  sym-

TABLE III. Measured Lorentzian-fitted Raman peak energies  $\omega_{\text{expt}}$  and full-width half-maximum linewidths  $\Gamma$  in  $\text{cm}^{-1}$ , corresponding calculated peak energies, and symmetries for the assigned modes in  $\text{Ti}_3\text{SiC}_2$ . Here, the asterisk refers to a mode for which the experimental peak width could not be determined.

Mode	$\omega_{\text{expt}}$	$\Gamma$	$\omega_{\text{calc}}$	Irrep.
(a)	159	10.5	145	$E_{2g}$
(b)	226	5.0	217	$E_{2g}$
(c)	279	5.6	253	$E_g$
(d)	301	*	301	$A_g$
	-	-	590	$E_g$
(e)	625	5.5	622	$E_{2g}$
(f)	673	4.7	657	$A_g$

metries, respectively, and are transverse and longitudinal modes involving adjacent C atomic planes. The mode predicted at 590  $\text{cm}^{-1}$  ( $E_g$ ) is not observed in our experiments. We note that the peak energies for our spectrum is in reasonable agreement with Ref. 7.

The 300-K Raman spectrum of  $\text{Ti}_4\text{AlN}_3$  (Fig. 3) exhibits eight distinct peaks of the ten expected for this structure. Experimentally fitted and calculated peak energies are compared in Table IV and show excellent agreement, though calculated modes at 248 and 255  $\text{cm}^{-1}$  are not observed in our spectrum.

Common to these phases is a lower energy ( $\sim 135\text{--}160\text{ cm}^{-1}$ ) shear mode principally involving the A planes. Each of these structures also exhibits one or more shear modes in the range of  $\sim 180\text{--}280\text{ cm}^{-1}$  involving both the M and A atomic planes. In structures with multiple X-group element layers, viz.,  $\text{Ti}_3\text{SiC}_2$  and  $\text{Ti}_4\text{AlN}_3$ , higher energy Raman-active modes are observed.

We remark that the intensities of the Raman peaks are somewhat surprising considering the absorption depth of these materials at the laser excitation wavelength is on the order of 10 nm.<sup>23</sup> The relatively long phonon lifetimes suggest that the MAX phases may be highly ordered and/or relatively defect free. Significantly, the narrow linewidths also suggest that the anharmonicity in these phases is relatively small as compared with other intermetallic systems; this is

TABLE IV. Measured Lorentzian-fitted Raman peak energies  $\omega_{\text{expt}}$  and full-width half-maximum linewidths  $\Gamma$  in  $\text{cm}^{-1}$ , corresponding calculated peak energies, and symmetries for the assigned modes in  $\text{Ti}_4\text{AlN}_3$ .

Mode	$\omega_{\text{expt}}$	$\Gamma$	$\omega_{\text{calc}}$	Irrep.
(a)	132	9.7	135	$E_{2g}$
(b)	181	7.6	172	$E_{2g}$
(c)	208	5.5	196	$E_g$
(d)	235	9.4	226	$E_g$
	-	-	248	$E_g$
	-	-	255	$A_g$
(e)	386	11.2	374	$A_g$
(f)	539	9.3	584	$E_{2g}$
(g)	563	7.9	587	$A_g$
(h)	592	10.6	600	$E_{2g}$

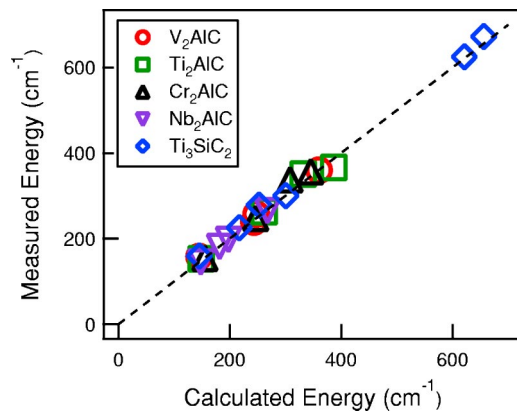


FIG. 4. (Color online) Correspondence of experimental and calculated energies for selected *MAX* phases.  $\text{Ti}_3\text{SiC}_2$  is denoted by blue (gray) diamonds,  $\text{Ti}_2\text{AlC}$  by green (gray) squares,  $\text{V}_2\text{AlC}$  by red (gray) solid circles,  $\text{Cr}_2\text{AlC}$  by upright black triangles,  $\text{Nb}_2\text{AlC}$  by inverted magenta (gray) triangles.

consistent, for example, with earlier reports of low coefficients of thermal expansion and high Debye temperatures.<sup>5</sup>

In general the identification of Raman modes with atom vibration is frequently used for identification of compounds, the measurement of residual stresses and the identification of

defects. In the *MAX* phases, because of their layered nature, we believe identification of the modes and correlating them with the database of physical and mechanical properties will be of vital and crucial importance for the rapid development of solid solution alloys. As noted above there are over fifty 211 phases and hence a correspondingly very large number of solid solution compositions indeed. By visualizing the modes, we can now correlate changes in the Raman frequencies directly with changes in bond energies between the various atoms and more importantly here between the layers.<sup>24</sup> As shown in Fig. 4, the agreement between measured and calculated Raman mode energies for all the structures reported here is excellent; a least mean squared linear fit of points shown in Fig. 4 yields a slope of  $0.992 \pm 0.005$ . This confirms the predictive capability of the *ab initio* method employed for the study of the lattice dynamics of these ternary carbides and nitrides.

We gratefully acknowledge Alexander Mavromaras and Paul Saxe from Materials Design for helpful discussions. This work was partially funded by the Division of Materials Research of the National Science Foundation (DMR-0072067) and ONR (N00421-03-0085). J.S. acknowledges partial support by ARO (YIP-W911NF-04-1-0308).

\*Author to whom correspondence should be addressed. Email address: spanier@drexel.edu

<sup>†</sup>Present address: Department of Mechanical and Materials Engineering, Wright State University, Dayton OH 45435.

<sup>1</sup>M. W. Barsoum, A. Murugaiah, S. R. Kalidindi, and T. Zhen, *Phys. Rev. Lett.* **92**, 255508 (2004).

<sup>2</sup>M. W. Barsoum, T. Zhen, S. R. Kalidindi, M. Radovic, and A. Murugaiah, *Nat. Mater.* **2**, 107–111 (2003).

<sup>3</sup>R. A. Guyer and P. A. Johnson, *Phys. Today* **52** (4), 30 (1999).

<sup>4</sup>R. A. Guyer, K. R. McCall, and G. N. Boitnott, *Phys. Rev. Lett.* **74**, 3491 (1995).

<sup>5</sup>M. W. Barsoum, *Prog. Solid State Chem.* **28**, 201 (2000).

<sup>6</sup>M. W. Barsoum and T. El-Raghy, *Am. Sci.* **89**, 336 (2000).

<sup>7</sup>M. Amer *et al.*, *J. Appl. Phys.* **84**, 5817 (1998).

<sup>8</sup>S. Gupta and M. W. Barsoum (unpublished).

<sup>9</sup>M. W. Barsoum, M. Ali, and T. El-Raghy, *Metall. Mater. Trans. A* **31A**, 1857 (2000).

<sup>10</sup>S. Gupta and M. W. Barsoum, *J. Electrochem. Soc.* **151**, D24 (2004).

<sup>11</sup>A. T. Procopio, T. El-Raghy, and M. W. Barsoum, *Metall. Mater. Trans. A* **31A**, 373 (2000).

<sup>12</sup>I. Salama, T. El-Raghy, and M. W. Barsoum, *J. Alloys Compd.* **347**, 271 (2002).

<sup>13</sup>M. W. Barsoum and T. El-Raghy, *Metall. Mater. Trans. A* **30A**, 363 (1999).

<sup>14</sup>G. Kresse and J. Furthmüller, *Phys. Rev. B* **54**, 11 169 (1996).

<sup>15</sup>K. Parlinski, Z. Q. Li, and Y. Kawazoe, *Phys. Rev. Lett.* **78**, 4063 (1997).

<sup>16</sup>Materials Design, Angel Fire, NM.

<sup>17</sup>G. Kresse and D. Joubert, *Phys. Rev. B* **59**, 1758 (1999).

<sup>18</sup>P. E. Blöchl, *Phys. Rev. B* **50**, 17 953 (1994).

<sup>19</sup>J. P. Perdew, K. Burke, and Y. Wang, *Phys. Rev. B* **54**, 16 533 (1996).

<sup>20</sup>Z. Sun, R. Ahuja, S. Li, and J. M. Schneiger, *Appl. Phys. Lett.* **83**, 899 (2003).

<sup>21</sup>E. H. Kisi, J. A. A. Crossley, S. Myhra, and M. W. Barsoum, *J. Phys. Chem. Solids* **59**, 1437 (1998).

<sup>22</sup>C. J. Rawn *et al.*, *Mater. Res. Bull.* **35**, 1785 (2000).

<sup>23</sup>S. Li H. Pettersson, C. G. Ribbing, B. Johansson, M. W. Barsoum, and R. Ahuja, *Appl. Phys. Lett.* (to be published).

<sup>24</sup>See EPAPS Document No. E-PRBMD0-70-109445 for animations of lattice displacements. A direct link to this document may be found in the online article's HTML reference section. The document may also be reached via the EPAPS homepage (<http://www.aip.org/pubservs/epaps.html>) or from <ftp.aip.org> in the directory /epaps/. See the EPAPS homepage for more information.